CHEMISTRY OF MATERIALS

Article

pubs.acs.org/cm

Colloidal Ordered Assemblies in a Polymer Shell—A Novel Type of Magnetic Nanobeads for Theranostic Applications

Nadja C. Bigall,[△,†] Claire Wilhelm,[‡] Marie-Lys Beoutis,[‡] Mar García-Hernandez,[§] Abid A. Khan,[∥] Cinzia Giannini,[⊥] Antoni Sánchez-Ferrer,[#] Raffaele Mezzenga,[#] Maria Elena Materia,[†] Miguel A. Garcia,[▽] Florence Gazeau,[‡] Alexander M. Bittner,[∥,^] Liberato Manna,[†] and Teresa Pellegrino[†,$,*]

[†]Istituto Italiano di Tecnologia, Via Morego 30, I-16163, Genova, Italy

[‡]Univ Paris Diderot, CNRS, UMR7057 Lab MSC, F-75205, Paris 13, France

[§]Instituto de Ciencia de Materiales de Madrid, CSIC E-28049, Madrid, Spain

[∥]CIC NanoGUNE Consolider Donostia San Sebastian E-20018, Spain

[^]Ikerbasque, 48011 Bilbao, Spain

[⊥]Istituto di Cristallografia, Consiglio Nazionale delle Ricerche, via Amendola 122/O, I-70126, Bari, Italy

[#]ETH Zürich, Institute of Food, Nutrition & Health, 8092 Zürich, Switzerland

[▽]Instituto de Cerámica y Consejo Vidrio, CSIC & IMDEA Nanociencia E-28049, Madrid, Spain

[$]Nanoscience Institute of CNR, NNL, Via Arnesano, I-73100 Lecce, Italy

Supporting Information

ABSTRACT: We present the synthesis of polymer embedded colloidal ordered assemblies, built from highly ordered superparamagnetic manganese iron oxide nanocrystals. Each assembly is wrapped into a thin polymer shell. In-depth characterization of the nanoparticles by TEM, SAXS, SQUID, and magnetophoresis indicates that these colloidal hybrids exhibit high mobilities in external magnetic fields, and that they could efficiently serve as contrast enhancers in magnetic resonance imaging.

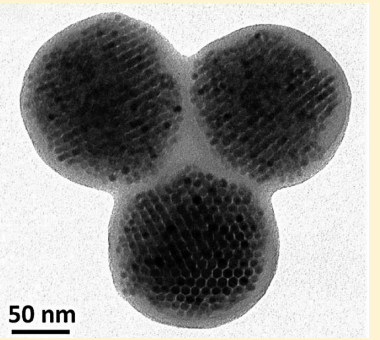

KEYWORDS: *colloidal assemblies, polymer shell, MRI contrast agents, magnetic nanoparticles*

INTRODUCTION

Colloidal Ordered Assemblies (COAs) from inorganic magnetic nanoparticles have only recently started to be investigated.[1] Mainly, they have been fabricated from materials such as silica and magnetite nanoparticles. Such particles are usually prepared by an elaborate treatment of micelle formation of nanoparticles, after dispersing droplets of the nanoparticle solutions in a nonsolvent, e.g., in the presence of dodecyltrimethylammonium bromide and poly(vinyl pyrrolidone). As far as the resulting physical properties are concerned, COAs have, for example, interesting magnetic properties, due to interparticle coupling, and hence different anisotropies.[2−6]

However, magnetic nanobeads (MNBs) from coprecipitated superparamagnetic nanoparticles, and amphiphilic polymers are materials of high interest in nanotechnology: potential applications are envisaged in magnetofection, cell separation, magnetically guided drug delivery and magnetically improved cell uptake, in hyperthermia and in magnetic resonance imaging (MRI).[7−15] The reason for the increasing interest in this type of materials is based on the simplicity of the fabrication process, and on the possibility to further functionalize the polymer toward fluorescence or cancer targeting. The pH dependence of the surface charge allows constructing carriers for cationic or anionic payloads.[7−9] More importantly, MNBs exhibit high magnetic moments, compared to the individual nanoparticles of which they are made. This originates from the synergy of the magnetic properties of several individual nanoparticles included within a single nanobead. As a consequence, these nano-objects exhibit high mobilities in external magnetic fields, while still being superparamagnetic, just like the individual nanoparticles of which they consist.[16,17] Presently, most types of MNBs consist of nonordered agglomerated nanoparticles.[7−9,12−15]

Here, we show a modification of a previously reported synthetic route developed by us for the synthesis of magnetic nanobeads, which leads to Polymer Encapsulated Colloidal Ordered Assemblies (polymer-COAs) with a substantial

Received: November 13, 2012
Revised: February 7, 2013
Published: February 12, 2013

dx.doi.org/10.1021/cm3036746 | *Chem. Mater.* 2013, 25, 1055−1062

improvement in terms of order of the nanoparticle assemblies inside the nanobeads. Our polymer-COAs exhibit exceptionally high mobility in external magnetic fields, and interesting magnetic properties, such as their Magnetic Resonance (MR) transversal relaxivity. By separating the aggregation step of the nanoparticles from that of the polymer condensation, it is possible to achieve colloidal close-packed ordered assemblies of the nanoparticles in a first step, and encapsulation of these colloidal ordered assemblies by a thin polymer shell in a final step.

The encapsulation by a few nanometer thick polymer shell allows us to exploit all the advantages of polymer nanobeads, including the possibility for further functionalization of the polymer. The thin polymer shell helps maintaining the structure of the ordered nanoparticle superstructures in a variety of hydrophilic environments, which is so far still challenging. We combine the high density (*fcc* packing) of the magnetic nanoparticles inside these objects with the increased colloidal stability based on the thin polymer shell of the polymer-COA.

Our polymer-COAs can find application as contrast agents in magnetic resonance imaging. In particular, we demonstrate that these new colloidal objects exhibit a distinct in vitro spin relaxation behavior, which is superior to that of corresponding MNBs made of nonordered magnetic nanoparticles. The high transversal relaxation rates of the COAs show nonlinear dependence on the concentration, which is a result of the high magnetic nanoparticle concentration inside the nanoobjects. Furthermore, as confirmed by magnetophoretic measurements, the high density of the magnetic materials results in an extremely high mobility of these polymer-COAs in magnetic gradient fields. The results suggest that the polymer-COAs are interesting candidates for applications requiring high mobility of magnetic nanoobjects, such as magnetically guided drug delivery, or magnetofection.

EXPERIMENTAL SECTION

Chemicals. Poly(maleic anhydride−*alt*−1-octadecene), M_n 30.000−50.000 (Aldrich), Milli-Q water (18.2 MΩ, filtered with filter pore size 0.22 μM) from Millipore, acetonitrile (HPLC grade, J. T. Baker) and tetrahydrofurane anhydride (Carlo Erba, p.a.), iron oxide hydroxide (Sigma Aldrich, #371254), iron acetylacetonate (Sigma Aldrich, 99%), manganese acetylacetonate (Sigma Aldrich, #245763), hexadecanediol (Sigma Aldrich, 90%), dodecylamine (Sigma Aldrich, 98%), lauric acid (Sigma Aldrich, 99%), benzyl ether (Sigma Aldrich, 98%), and octadecene (Sigma Aldrich, 90%), were used without any further purification.

Synthesis of Manganese Iron Oxide Nanoparticles. Manganese iron oxide nanoparticles were prepared following previous works.[18] After mixing 2 mmol iron acetylacetonate, 1 mmol manganese acetylacetonate, 10 mmol hexadecanediol, 6 mmol dodecylamine, 6 mmol lauric acid, and 20 mL benzyl ether, the solution was exposed to a flow of nitrogen and heated to 140 °C for 1 h, then to 210 °C for 2 h and finally to 300 °C for one more hour. Subsequently, the samples were washed several times using ethanol, acetone, and isopropanol as precipitation agents and centrifugation, followed by redispersion in toluene.

Synthesis of Iron Oxide Nanoparticles. Iron oxide nanoparticles were prepared following the method published by Colvin et al. recently.[19] Briefly, 0.18 g iron oxide hydroxide, 2.3 or 3.45 g oleic acid (leading to a ratio of oleic acid to iron oxide hydroxide of 4 or 6, respectively) and 5 g octadecene were transferred to inert gas atmosphere and stirred at 320 °C for 1 h. Finally, the nanoparticles were washed twice by the addition of ethanol or methanol as nonsolvent followed by centrifugation, removal of the supernatant and redissolution in fresh toluene.

Synthesis of Colloidal Ordered Assemblies. In a typical synthesis, 0.1 nmol manganese iron oxide nanoparticles were dried and redissolved in 200 μL tetrahydrofurane. After vortexing at 1000 rpm for 30 min, 0.8 mL acetonitrile were added at a rate of 250 μL min^{-1}.

Synthesis of Polymer Embedded Colloidal Ordered Assemblies (polymer-COA). Typically, 0.08 nmol manganese iron oxide nanoparticles were dried and redissolved in 190 μL tetrahydrofurane. After vortexing at 1000 rpm for 15 min, 0.2 mL acetonitrile were added with a rate of 250 μL/min to form colloidal ordered assemblies, and the sample was further vortexed for five minutes. Subsequently, a solution consisting of 1.5 μmol monomers of poly(maleic anhydride−alt−1-octadecene), 200 μL tetrahydrofurane and 300 μL acetonitrile was added to the colloidal assemblies, followed by vortexing the mixture for another five minutes. Finally, 1.2 mL of acetonitrile was added at a rate of 125 μL min^{-1}. A few drops of water were added to increase the stability of the product (by opening the anhydride rings, the surface charge increases, hence agglomeration can be reduced), before the polymer-COAs were separated from the solution through an external magnetic gradient field. The polymer-COA could be easily redispersed in Milli-Q water for further characterization.

Synthesis of Original Magnetic Nanobeads (MNBs). As a comparison, original MNBs were prepared following previously published methods.[8,9] In our case, the same amount of nanoparticles as used for the polymer-COAs was dried and redissolved in tetrahydrofurane, followed by the addition of the same amount of poly(maleic anhydride−alt−1-octadecene) as used for the polymer-COA, so that the final solution had a total volume of 0.2 mL. After vortexing for 30 min, 0.8 mL of acetonitrile were added at a rate of 250 μL min^{-1}. By placing a magnet beside the vial overnight, the MNB could be separated from the solution and redispersed in Milli-Q water.

Elemental Analysis. An inductively coupled plasma atomic emission spectrometer (ICP-AES, iCAP 6500, Thermo) was used for determining the concentration of the nanoparticles by elemental analysis. The samples were prepared by drying an aliquot of the sample under air flow and dissolving it in 0.5 mL of aqua regia overnight. Subsequently, the sample was diluted with deionized water to a final volume of 25 mL.

TEM Characterization. Transmission electron microscopy was carried out on a JEOL JEM-1011 apparatus with an acceleration voltage of 100 kV. The sample preparation was conducted by dropcasting a droplet of the sample onto a carbon coated copper grid with subsequent removal of the liquid by evaporation under ambient conditions.

SAXS Characterization. SAXS data were collected at the XMI-LAB facility in Bari, equipped with a X-ray synchrotron class rotating anode microsource (Rigaku FR-E+ SuperBright) coupled, through a focusing high-flux multilayer optics, (Cu Kα radiation) to a three-pinhole camera (SMAX-3000) for the simultaneous acquisition of 2D micro SAXS-WAXS data in scanning mode. The system is equipped with two 2D distinct detectors: Triton20 gas-filled proportional counter SAXS detector, 20 cm in diameter and 100 μm pixel size, and RAXIA image plate WAXS detector with off-line read-out unit and 100 μm pixel size. Data were acquired for a total integration time of 2 h, using a focal spot at the sample position (circular shape) ∼0.2 × 0.2 mm^2. Solutions were inserted in 0.7 mm glass capillaries. The fitted curves were obtained following the expression $I(q) = f \cdot P(q) \cdot S(q)$, where $P(q)$ is the form factor of the sphere and $S(q)$ is the supercrystalline structure factor for a face-centered cubic structure (*fcc*), as justified by TEM images already. The parameter f takes into account the corresponding scattering length density of the nanoparticles $\rho_{NPs} = 4.20 \times 10^{-5}$ $Å^{-2}$ and of the matrix $\rho_{polym} = 9.13 \times 10^{-6}$ $Å^{-2}$ or $\rho_{ACN} = 7.09 \times 10^{-6}$ $Å^{-2}$.[20,21] For a supercrystalline structure with layering distance D, a nonperfect packing of the single nanoparticles is expected due to their inherent polydispersity. Thus, a distortion factor $g \approx \Delta D/D$ of the supercrystal is included in the calculation of $S(q)$. For an *fcc* phase the lattice parameter a can be calculated through the relation $a = \sqrt{2} \cdot D$.

SQUID Characterization. Magnetization curves at low temperature (5 K) and at room temperature of the suspensions were measured in the range from −50 kOe to +50 kOe using a

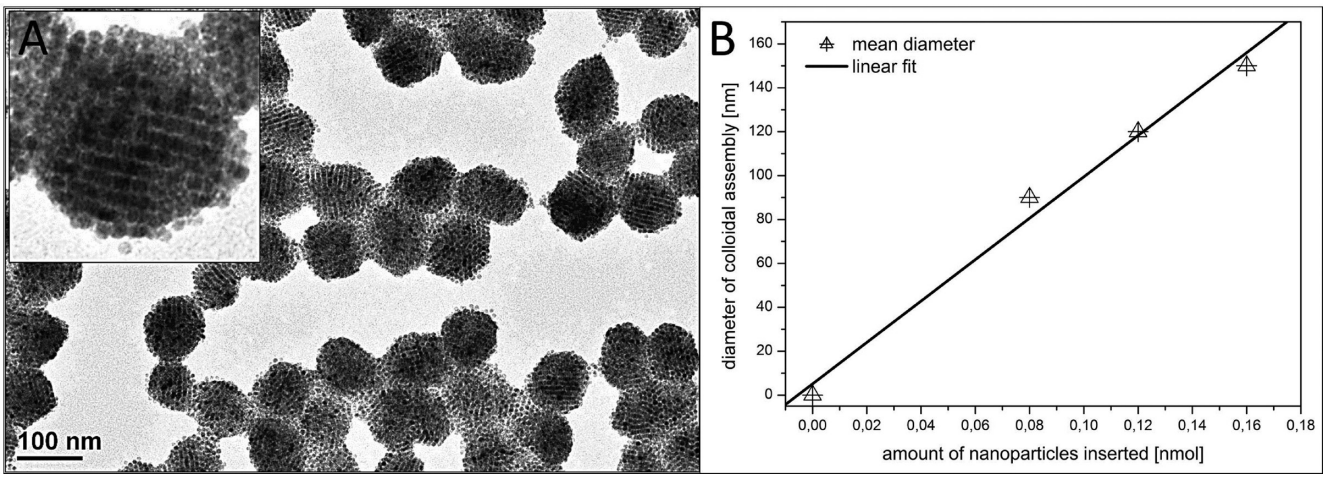

Figure 1. (A) TEM images of COAs in high (inset) and medium magnification and (B) diameter of the COAs plotted versus the initial amount of nanoparticles as obtained from TEM measurements.

superconducting quantum interference device (SQUID) from Quantum Design with a homemade Teflon liquid sample holder. Thermal dependence of the magnetizations were also measured in Zero Field Cooling (ZFC) and Field Cooling (FC) runs by applying a cooling field of $H_{cooling}$ = 50 kOe and a magnetic field of H_{meas} = 50 Oe during the measurement. For all magnetic measurements, the diamagnetic contribution of the sample holder has been subtracted. Any possible magnetic contribution from the sample holder (that we have measured separately) was at least 3 orders of magnitude smaller than that of the sample.

Magnetophoretic Mobilities of the COAs and MNBs. To derive the magnetophoretic potential of each sample, a magnetic attractor was used.[22] It consisted of a 50 μm diameter nickel wire placed in a chamber submitted to a 0.2 T magnetic field (which saturates the magnetization of the nanoobjects). The magnetic field gradient developed in proximity of the wire was carefully calibrated using 1 μm beads (Dynabeads, MyOne). Individual nanoobjects attracted to the wire were tracked when passing through an observation window situated at a distance of 50 μm apart from the wire extremity. At this distance, the magnetic field gradient ∂_xB equals 365T/m. The viscous drag force acting of the migrating nanobeads, given by $3\pi\eta d_{hyd}v$ (η being the fluid viscosity 10^{-3}Pa·s, d_{hyd} the hydrodynamic diameter of the nanobead as measured by DLS and v its measured velocity), equals the magnetic force $\mu\partial_x$B (μ being the nanobead magnetic moment at saturation). This magnetic moment μ is therefore directly inferred from the value of the velocity. Such measurements are averaged over 100 nano-objects and repeated three times. To compare the different samples in terms of the magnetic targeting potential, it is convenient to define a single parameter k that predicts the magnetic velocity for a given magnetic field gradient and surrounding viscosity:

$$k = \mu/(3\pi d_{hyd})$$

with k being expressed as m/s * $(T/m)^{(-1)}$ * Pas. This parameter can be seen as a magnetic relative mobility and varies with the squared diameter of the nanoobjects.

MR Relaxometry Characterization. The relaxation times were measured at 0.47 T (20 MHz proton Larmor frequency) and 37 °C using a Minispec PC120 spectrometer (Bruker, France). The T_1 relaxation time was calculated from the inversion−recovery sequence, with 15 data points and 3 acquisitions for each measurement. The T_2 relaxation time was obtained from a Carr−Purcell Meiboom Gill (CPMG) spin−echo pulse sequence (100 data points, 3 acquisitions). T_1 and T_2 were determined three times for each sample with standard deviations of 2% and 5%, respectively.

RESULTS AND DISCUSSION

Figure 1(A) shows Transmission Electron Microscopy (TEM) images of the COAs dried on a TEM grid, as overview, and in higher magnification (inset). The COAs are nearly spherical, and to a certain degree still ordered after the deposition on the copper grid, even though some free nanoparticles can be additionally found on the same grid. In the absence of an external magnetic field, the dispersion of the COAs was stable in solution for several weeks, and the COAs could even be redispersed after settling. When the COAs were dried in an applied external magnetic field (0.3 T), they followed the magnetic field lines (see Supporting Information, SI, Figure SI1), while maintaining their shape. However, by drying the COA and adding fresh tetrahydrofurane (THF), we were able to destroy the superstructures, and to restore the pristine nanoparticle solution (see SI Figure SI2). Generally, we found that the more destabilizing solvent (acetonitrile) we added during the preparation, the more stable the COAs were upon drying on a TEM grid. Also the size and shape of the products strongly depended on the type of destabilizing agent; the best results were obtained using acetonitrile (a comparison of various destabilizing agents is shown in the SI Figure SI3). However, the size of the COAs obtained upon adding a certain amount of acetonitrile scaled with the initial nanoparticle concentration. For example, it was observed that 160 pmol nanoparticles yielded stable COAs when 0.1 mL acetonitrile was added, while under the same conditions 40 pmol nanoparticles lead to a side product made of micelle-type agglomerates only (see SI Figure SI4). In total, the dependence of the diameter of the COAs on the amount of initial nanoparticles was nearly linear in the investigated parameter range (Figure 1B).

In our previous works, manganese iron oxide nanoparticles had been coprecipitated in the presence of an amphiphilic polymer to yield MNBs consisting of agglomerated nanoparticles in the core surrounded by a polymer shell using acetonitrile as destabilization agent.[7−9] For a TEM image of a typical MNB sample please see SI Figure SI5b,c, while the nanoparticles which were the building blocks for the MNBs and COAs are reported in Figure SI 5a.[7−9] In the present work, we achieved highly ordered nanocrystal superstructures within the COAs when, in absence of the polymer, the destabilization agent (acetonitrile) was added to the magnetic nanocrystals

dx.doi.org/10.1021/cm3036746 | Chem. Mater. 2013, 25, 1055−1062

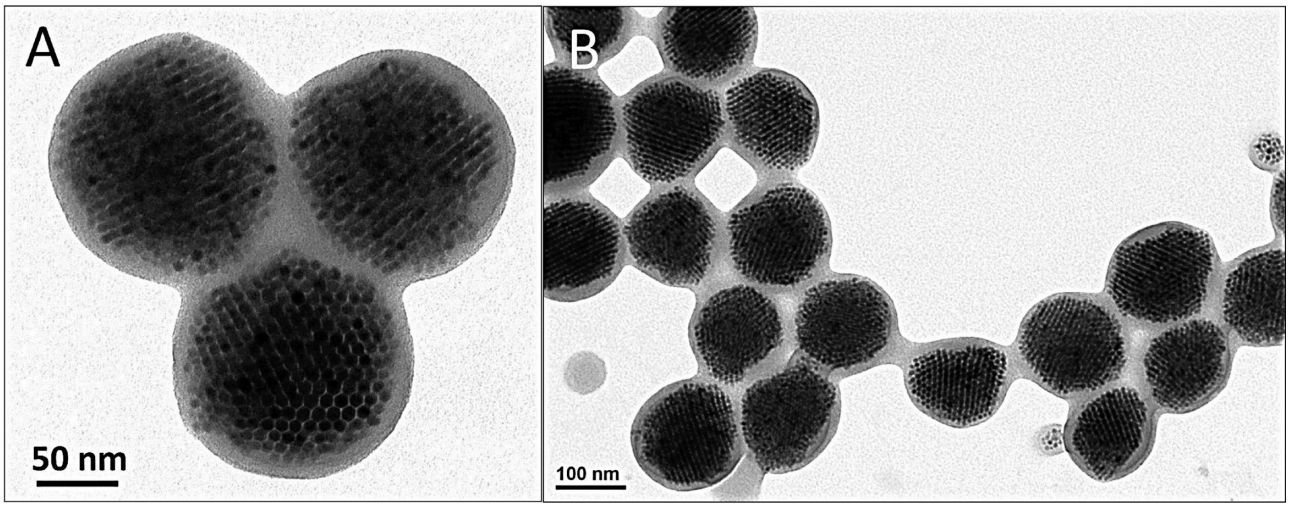

Figure 2. TEM images of polymer-COA at higher (A) and lower (B) resolution. The dark pattern (A) results from the ordering of the closed packed assemblies within the nanobeads, while the brighter gray ring is caused by the polymer shell (lower electron density) of around 20 nm thickness.

dissolved in THF. Solubility tests also revealed that the formation of stable COAs occurs when we added a volume of acetonitrile such that the polymer was still sufficiently soluble (polymer beads cannot form at these added volumes of acetonitrile, see the SI). As a consequence, in the next step poly(maleic anhydride−alt−1-octadecene), dissolved in a mixture of acetonitrile and THF, was added to the preformed colloidal assemblies, followed by further slow addition of acetonitrile, so that the destabilized polymer could condense onto the assemblies which acted as seeds. The resulting colloid was easily separable from solution by external magnetic gradient fields and redispersible in water. On the contrary, the bare COAs, without polymer at their surface, decomposed upon exposition to the magnetic field. Fourier transform infrared spectroscopy (FT-IR) characterization carried out on those samples (see SI Figure SI 6) and also previous works showed that the exposure of this polymer to water opens some of the anhydride groups, so that the resulting nano-objects are negatively charged in water. This was also confirmed by zeta potential measurements (see SI): indeed the electrostatic repulsions prevent them from aggregation.[7−9] A typical TEM image of the resulting polymer-encapsulated Colloidal Ordered Assemblies (polymer-COAs) is shown in Figure 2. Remarkably, the nanoparticles within the polymer shell appear to be much more ordered than in absence of the polymer. This could mean that the COAs, in absence of polymer, are partly destroyed during the drying process of the TEM grid preparation. Alternatively, due to the solvation of the polymer, additional depletion attraction forces[23] drive the already assembled particles into an even more ordered state. The polymer shell around the polymer-COA, of ca. 20 nm, is relatively thin in comparison to the polymer-COA diameter of 120−140 nm as measured by TEM (Figure 2).

It should be mentioned that, by following the same destabilization route, we were also able to successfully synthesize polymer-COA from superparamagnetic nanoparticles of a different material (magnetite nanoparticles of Fe_3O_4, synthesized as described by Yu et al.).[19] For TEM images of these nanoparticles and of the resulting polymer-COAs, see SI Figure SI7. Even in this case, the dispersion of the COA was stable for only a few minutes, and only the resulting polymer-COA were long-term stable again. In the following, 70 nm diameter COAs (**sample H**) and 96 nm diameter COAs (**sample G**), as well as 119 nm-diameter polymer-COAs (**sample D**) and 134 nm diameter polymer-COAs (**sample F**), are characterized and compared with conventional MNBs, obtained from the same nanocrystal solution following our previously reported procedure[9] (**sample E**, 45 nm ±10 nm) (see Table 1 and SI Figure SI 8). The corresponding

Table 1. Four Different Samples Characterized Including the Inserted Amount of Manganese Iron Oxide Nanoparticles and Polymer Inserted during the Synthesis, As Well As the Average Outer Diameter As Obtained from TEM Analysis

sample name	# nanoparticles (nmol)	# polymer (in monomer units)	outer diameter
COA (H)	0.08	0	70 ± 21 nm
COA (G)	0.1	0	96 ± 24 nm
polymer-COA (D)	0.1	1.5 μmol	119 ± 34 nm
polymer-COA (F)	0.08	1.5 μmol	134 ± 21 nm
MNB (E, reference)	0.1	1.5 μmol	45 ± 10 nm

hydrodynamic diameters measured by dynamic light scattering (DLS) also confirmed for those samples a good stability in solution, with a narrow size distribution. Comparison between the corresponding samples with and without polymer shell confirmed the enlargement of the diameters of the nanobeads in the presence of the shell (SI Figure SI9).

In order to investigate the structural features of the assemblies in more detail, we acquired 1D small-angle X-ray scattering (SAXS) patterns of the polymer-COAs (samples D and F) and of the 96 nm COAs (sample G). These are shown in Figure 3. All of the obtained values from the fitting curves for the three samples are summarized in Table 2. From the fitted curves, the average diameters (d) of the three samples are in the same range—from 8.1 to 8.3 nm, as well as the distortion factors (g)—an indication of similar packing. The main differences appear on the distance between neighboring nanoparticles (D) and the corresponding lattice parameter (a). For the COA (sample G) the average distance between nanoparticles is D = 8.5 nm (a = 12.0 nm), while for the polymer-COA (samples D and F) this average distance is D = 9.3 (a = 13.2 nm) and 9.7 nm (a = 13.8 nm), respectively. This

dx.doi.org/10.1021/cm3036746 | Chem. Mater. 2013, 25, 1055−1062

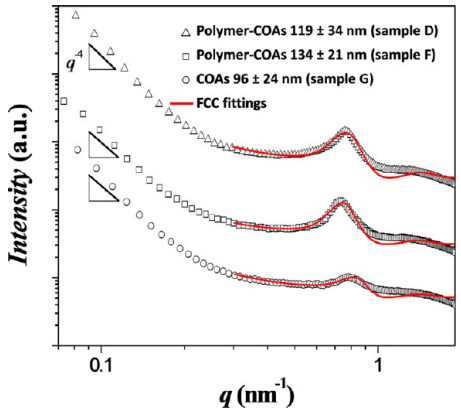

Figure 3. 1D SAXS scattering curves and their corresponding fitting curves for the polymer-COAs of 119 nm outer diameter (sample D), the polymer-COAs of 134 nm outer diameter(sample F), and COAs of 96 nm diameter (sample G). An offset was chosen in order to visualize better all three scattering curves.

increase in the distance between nanoparticles might be due to the presence of polymer molecules interacting with the surface of the nanoparticles, which would build up a polymeric layer of more than 0.5 nm in thickness. The q^{-4} slope measured for the scattered intensity at lower scattering vectors ($q \leq 0.1$ nm^{-1}, corresponding to characteristic length scales $\geq$60 nm) is indicative of Porod scattering,[24] typical for sharp interfaces: this is consistent with the presence of large superstructures, as shown in the TEM images, ranging from 50 nm to more than 100 nm.

The formation of *fcc* close-packed assemblies may induce modifications in the magnetic properties of the nanoparticles due to dipolar interactions.[25,26] In order to confirm this point, we performed a study of the magnetic properties of the initial nanoparticles and of the various types of assemblies. Magnetic measurements at 5 K (not shown) identified a paramagnetic component below 5% of the ferromagnetic signal, presumably corresponding to a certain leakage of iron ions. However, at room temperature, this contribution was smaller than the noise signal and therefore negligible. Figure 4a presents the magnetization curves at 300 K of the liquid samples. Eight nm nanoparticles would be expected to be purely superparamagnetic at 300 K only if two requirements are fulfilled: (i) They must act completely isolated from each other. This condition is mostly fulfilled for the colloidal assemblies, since the measurements were conducted in solution so that the nanoparticles were not in close contact to each other; (ii) The other condition would be that the effective anisotropy should be that of the bulk maghemite. This, however, is usually not the case. Surface effects increase the effective anisotropy of small nanoparticles (as shown for example by Song et al.)[27] and other effects like surface spin glass or spin canting can also explain the small observed hysteresis. Note that the ZFC curves decrease above the blocking temperature but they still have appreciable values at 300 K that account for the existence of a small hysteresis.

The curves show similar profiles with similar saturation fields and slopes of the magnetization curves at low fields. However, the detail of the low field region (inset in Figure 4a) shows some differences between the assemblies. The curve corresponding to the individual nanoparticles is indicative of superparamagnetic behavior, whereas the assemblies exhibit room temperature coercivity due to interparticle interactions.[25] Small COAs (sample H with diameters of 70 ± 21 nm) show a coercivity of the order of 10 to 15 Oe, which is close to the resolution of the measurement, but increasing the size (sample G) leads to a higher coercivity. The polymer-COAs (samples D and F) show coercivities decreasing with the size of the nanoobjects. According to the literature, when magnetic nanoparticles are close enough they exhibit dipolar interactions that modify their magnetic properties.[26−28] For disordered ensembles of nanoparticles, these interactions commonly induce an increase of the coercivity, as we observed here.[26] However, for ordered ensembles of nanoparticles it has been found that dipolar interactions reduce the coercivity, which is consistent with our present observations.[27,29] This effect described in literature is also observed in our ordered assemblies. When the magnetic moment of a nanoparticle is reversed, it triggers the reversal process of the neighboring nanoparticles through dipolar interactions; these interactions are such that the 134-nm polymer-COA (sample F) require smaller fields for saturation than the conventional MNBs (sample E) and the COAs (samples H and G).

Further assessment of the magnetic properties of the assemblies was obtained by measuring the thermal dependence of the magnetic susceptibility, see Figure 4b and SI Figure SI10. All curves correspond to blocking temperatures (TB) below 80 K. Noteworthy, the highest TB corresponds to isolated NPs with a value of 60 K, while the polymer-COA present TB in the range of 35−40 K and the COA in the range of 30−35 K. Our results suggest that the dipolar coupling between the ordered nanoparticles reduces the energy barrier that keeps the nanoparticles blocked, and hence reduces the blocking temperature. These observations are in good agreement with those from references.[28,29] However, for completeness, it should be stated that there are controversial opinions on this issue.[31]The dipolar interactions are limited to the first neighbors. Thus, the effect of interparticle interactions is weakly dependent on the supercrystal size.

It is necessary to rule out the possibility that these differences could be related to some changes in the electronic structure of the nanoparticles (the ultimate responsible of the magnetic properties) induced during the fabrication of the COAs and polymer-COAs. Therefore, we performed a study of the

Table 2. Average Diameter (d) of the Single Nanoparticles, Distortion Factor (g), Layering Distance (D) and Lattice Parameter (a) Obtained from the SAXS Fitting Curves of the Three Different Samples D, F, and G

sample name and diameter from TEM	d (nm)	g	$D \pm \Delta D$ (nm)	$a \pm \Delta a$ (nm)
polymer-COAs of 119 nm (sample D)	8.13	0.155	9.30 ± 1.02	13.15 ± 1.44
polmer-COAs of 134 nm (sample F)	8.31	0.143	9.74 ± 0.99	13.78 ± 1.40
COAs of 96 nm (sample G)	8.29	0.157	8.45 ± 0.94	11.95 ± 1.32

dx.doi.org/10.1021/cm3036746 | *Chem. Mater.* 2013, 25, 1055−1062

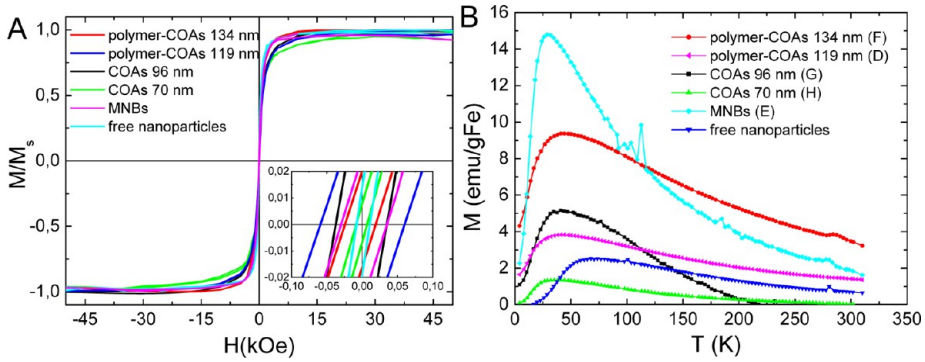

Figure 4. (a) Normalized magnetization curves measured at RT. The inset represents a detail of the low field region and (b) thermal dependence of the magnetization upon zero field cooling (H_{meas} = 50 Oe).

samples electronic structure by means of X-ray absorption spectroscopy (XAS) at the Fe K edge. Measurements were carried out at the BM25 (SpLine) beamline in ESRF, Grenoble France. The results, shown in the SI Figure SI11, confirmed that both for the conventional MNBs and for the COAs or polymer-COAs the changes in electronic structure should be negligible, as they could not be detected by XAS.

Hence, we can conclude that even though the magnetic moment for the assembly is not larger than the sum of the moments of the individual particles, the advantage of the assembly is that we have achieved a very large magnetic moment per nano-object (the sum of those of the individual nanoparticles), while, at the same time, no significant variations in the superparamagnetic behavior of the nanoparticles are induced, so that the nano-objects are almost superparamagnetic. These slight differences are induced by interparticle interactions that can be tuned through the assembly size and ordering.

In Figure 5, the MR relaxation rates of two differently sized polymer-COA samples are shown, as well as the relaxation rates of conventional MNBs synthesized with a similar amount of nanoparticles and polymer. For comparison, also the relaxation rates of free nanoparticles in water, transferred with the same polymer using the water transfer procedure as described in ref 30 are measured. The slope of the linear curve of the inverse

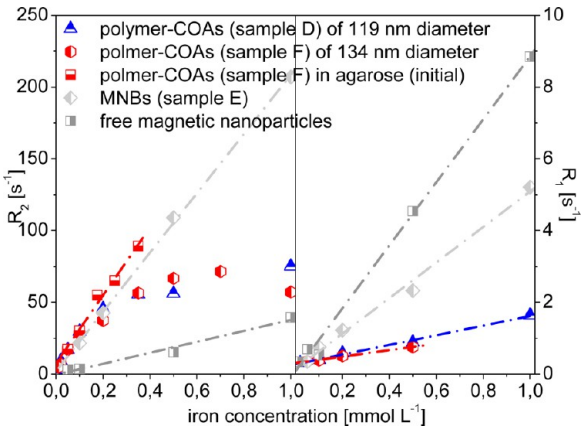

Figure 5. Relaxation rates (right) R_1 and (left) R_2 (inverse relaxation times T_1^{-1} and T_2^{-1}) depending on the concentration of iron. Presumably, the nonlinear dependency for the polymer-COAs comes from chain formation in the external magnetic field, which is reasonable since the polymer-COAs exhibit exceptional high magnetophoretic mobilities.

relaxation times T_1 and T_2 versus the sample concentration represents the concentration-independent relaxivity. As expected from previous works on assembled or encapsulated nanoparticles,[11,12,31,32] the assemblies investigated here show low R_1 longitudinal relaxivity and instead high R_2 transverse relaxivity. In comparison, the R_1 relaxivities are highest for the free nanoparticles with 10 mM^{-1} s^{-1}, followed by the MNB relaxivity with 5 mM^{-1} s^{-1}. The R_1 relaxivity of the 119 nm diameter polymer-COA is with 1.3 mM^{-1} s^{-1} slightly higher than the relaxivity of the 134 nm diameter polymer-COA with a value of 0.9 mM^{-1} s^{-1}. From the R_2 relaxation curves it can be derived that, as expected, the free nanoparticles again show the smallest r_2 relaxivities with 38 mM^{-1} s^{-1}, followed by the relaxivity of the MNB with 177 mM^{-1} s^{-1}. The relaxation rates of the polymer-COA samples, however, show a nonlinear behavior with a very steep slope for small concentrations and saturation for higher iron concentrations (Figure 5 left). The initial slope of the 119 nm diameter polymer-COA is smaller than the one of the 134 nm diameter polymer-COA. To further investigate this effect, we repeated the T_2 measurements of the 134 nm diameter polymer-COA after embedding them in a 0.3% agarose gel, a denser medium (red squares in Figure 5 left). In this case, at least at the beginning of the measurements we observed a nearly linear relaxation dependence on the concentration, indicating a relaxivity of 236 mM^{-1} s^{-1}. With exposure to the magnetic field of the setup (0.47T), however, the values for higher iron concentrations decrease again (see SI Figure SI12). This observation is an indication of chain formation or aggregation of the polymer-COA when exposed to an external magnetic field. The polymer-COA are moving faster than the free manganese iron oxide nanoparticles (see section below) and faster than the conventional MNBs due to the high packing of the nanoparticles. Therefore, the formation of chains in the polymer-COA system is much easier than in the reference samples (in which, within the same time frame of the measurements, no such effect is observed). Due to the *fcc* closed packing of the nanocrystals and the thin polymer shell, the MRI R_2 contrast properties are optimized, since the resulting polymer-COA nano-objects exhibit a high global magnetic moment, are still superparamagnetic and do not agglomerate in the absence of an external magnetic field. Moreover, as shown in our previous works about MNBs, nano-objects prepared using poly(maleic anhydride−alt−1-octadecene) exhibit negative surface charge, so that, due to electrostatic repulsion, the polymer-COA are stable in aqueous solution.[7,9,30,33] In contrast, during MRI measurements, an external magnetic field is applied. In this case, the magnetic field

dx.doi.org/10.1021/cm3036746 | *Chem. Mater.* 2013, 25, 1055−1062

induced in the polymer-COA is remarkably high due to the highest possible nanoparticle density as a result of the *fcc* packing. However, the polymer shell is still thin enough to allow water molecules to get in close proximity to the induced magnetic inhomogeneity of the polymer-COA, which is again favorable for fast dephasing of the proton spins and, hence, large R_2 relaxivities. The exceptional high mobilities of the polymer-COAs were also confirmed by magnetophoretic measurements. Figure 6a and b show the covering of the

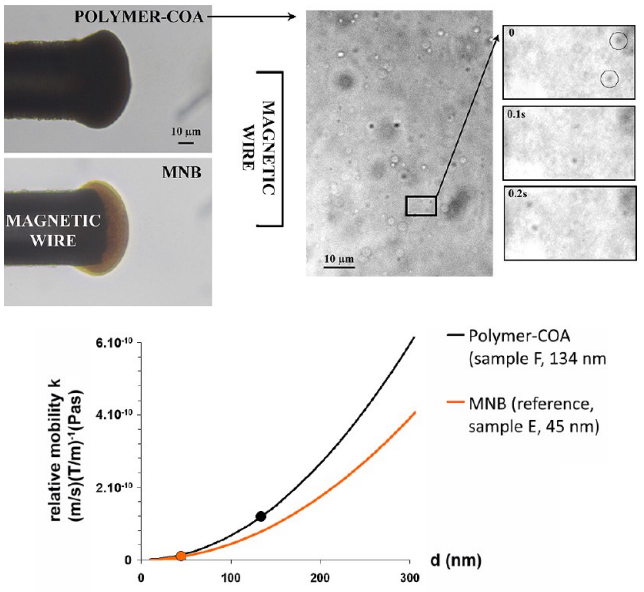

Figure 6. Magnetophoretic measurements of polymer-COAs in comparison to normal MNB. Observation at 20× magnification with color camera of the magnetic tips covering with polymer-COAs or MNB (top, left), and observation at 100× magnification with a high resolution CoolSNAP HQ2 camera of a typical zone 50 μm apart from the magnetic wire (top, right). In such case, the nanoparticles are clearly identified and can be easily tracked (see the zoomed sequence of images at 0.1 s time interval) to infer magnetophoretic mobility. Relative mobility k as a function of the diameter (bottom panel).

magnetic attractor upon application of the magnetic field. Interestingly, the 134-nm polymer-COAs (sample F) appear much darker, probably reflecting the higher loading with magnetic nanoparticles. Magnetophoretic velocities of the MNP (sample E) and the 134 nm polymer-COA (sample F) were found to be (3.2 ± 0.4) μm/s and (43.1 ± 2.5) μm/s, respectively. Hence, the respective magnetic moments were calculated to be (5.6 ± 0.8)10−18 Am^2 and (2.3 ± 0.3)10−16 Am^2. To compare the different materials, the magnetophoretic parameter k defined in the Experimental Section (and expressed as $(m/s)(T/m)^{-1}(Pas)^{-1}$) was computed as a function of the size. The plot showing the predicted and measured relative magnetic mobilities versus particle size is shown in Figure 6c for the different materials. A higher mobility of the polymer-COA versus the standard MNBs is certainly observed.

CONCLUSIONS

We have presented a route to prepare *fcc* colloidal ordered assemblies from manganese iron oxide nanoparticles, which were subsequently enwrapped into a passivating polymer shell of about 10 to 20 nm thickness that provides stability in an aqueous environment. To achieve such control, it was crucial to separate the destabilization of nanoparticles from that of the polymer. To this aim, rather than starting with a mixture containing both the polymer and the nanoparticles to be destabilized at the same time by solvent addition, as previously reported by us,[8,9] here we first destabilized a solution of nanoparticles. Then, in a second step, we added the polymer solution to be destabilized. As a result, controlled ordering of the nanoparticles occurred in the first step, and in the second step polymer embedding of the preformed ordered clusters took place. Remarkably, with the polymer shell, these ordered assemblies are mechanically stabilized in solution and can be easily transferred to other solvents like, e.g., water, hence find applications in nanomedicine. Superparamagnetic behavior, ordering of closed packed nanoparticles, and high mobility under external magnetic fields for the polymer-COAs were proven by different techniques. The closed packing of the nanoparticles within the polymer-COA and the thin stabilizing polymer shell allow for high R_2 relaxation rates which were, only for low iron concentrations, linear with the iron concentration. For Fe concentrations higher than 0.3 mmol L^{-1} a nonlinear concentration dependency of the R_2 relaxation rates was found, which was attributed to chain formation in external magnetic fields. These results clearly illustrate the potential of the polymer-COAs for applications requiring high mobility in magnetic field gradients such as magnetically guided drug-delivery or magnetofection, as well as for valuable contrast agents working with high sensitivity at low doses, and at the same size of the standard nanobead (100−200 nm in diameter). Future experiments will follow aiming at a broad functionalization of the polymer-COA by exploiting the functional groups of the polymer.

ASSOCIATED CONTENT

Supporting Information

Properties of COAs and polymer-COAs, assembly under magnetic fields, influence of solvents and concentrations; TEM images of nanoparticles, MNBs, and of polymer-COAs from different magnetic nanoparticle material; TEM images of the investigated samples, relaxation rates in agarose and water, as well as XAS, FT-IR, and DLS spectra and the data from magnetic FC measurements. This material is available free of charge via the Internet at http://pubs.acs.org.

AUTHOR INFORMATION

Corresponding Author

* E-mail: teresa.pellegrino@unile.it.

Present Address

△Physikalische Chemie und Elektrochemie, Callinstr. 3, 30167 Hannover, Germany.

Notes

The authors declare no competing financial interest.

ACKNOWLEDGMENTS

This work was supported in part by the European projects Magnifyco (contract no. NMP4-SL-2009-228622) and the starting ERC grant NANO-ARCH (contract no. 240111), by the Italian FIRB projects (Nanostructured oxides, contract no. 588 BAP115AYN) and ("Rete integrata per la Nano Medicina (RINAME)" − RBAP114AMK_006) and by the IIT SEED Project XMI-LAB (grant no. 21537), as well as by MEC and Consejo Superior de Investigaciones Científicas (PE-2010 6 0E 013). The authors would like to thank A. Espinosa and A.

Muñoz for the assistance with the experiments and O. Clément and G. Autret for giving access to the MR relaxometer. We acknowledge the European Synchrotron Radiation Facility for provision of synchrotron radiation facilities and the MEC and Consejo Superior de Investigaciones Científicas for financial support (PE-2010 6 0E 013) and for provision of synchrotron radiation facilities, and we would like to thank the BM25-SpLine staff for the technical support.

■ ABBREVIATIONS

COAs, colloidal ordered assemblies; MNBs, magnetic nanobeads; polymer-COAs, polymer embedded colloidal ordered assemblies

■ REFERENCES

(1) Rogach, A. L.; Talapin, D. V.; Shevchenko, E. V.; Kornowski, A.; Haase, M.; Weller, H. *Adv. Funct. Mater.* **2002**, *12*, 653.
(2) Wang, D.; Xie, T.; Peng, Q.; Li, Y. *J. Am. Chem. Soc.* **2008**, *130*, 4016.
(3) Zhuang, J.; Wu, H.; Yang, Y.; Cao, Y. C. *Angew. Chem., Int. Ed.* **2008**, *47*, 2208.
(4) Cho, Y.-S.; Yi, G.-R.; Kim, S.-H.; Pine, D. J.; Yang, S.-M. Y. *Chem. Mater.* **2005**, *17*, 5006.
(5) Pileni, M. P. *Langmuir* **1997**, *13*, 3266.
(6) Zhuang, J.; Wu, H.; Yang, Y.; Cao, C. Y. *J. Am. Chem. Soc.* **2007**, *129*, 14166.
(7) Bigall, N. C.; Curcio, A.; Leal, M. P.; Falqui, A.; Palumberi, D.; Di Corato, R.; Albanesi, E.; Cingolani, R.; Pellegrino, T. *Adv. Mater.* **2011**, *23*, 5645.
(8) Di Corato, R.; Bigall, N. C.; Ragusa, A.; Dorfs, D.; Genovese, A.; Marotta, R.; Manna, L.; Pellegrino, T. *ACS Nano* **2011**, *5*, 1109.
(9) Di Corato, R.; Piacenza, P.; Musaro, M.; Buonsanti, R.; Cozzoli, P. D.; Zambianchi, M.; Barbarella, G.; Cingolani, R.; Manna, L.; Pellegrino, T. *Macromol. Biosci.* **2009**, *9*, 952.
(10) Bigall, N. C.; Parak, W. J.; Dorfs, D. *Nano Today* **2012**, *7*, 282.
(11) Min, H. S. C.; Liong, M.; Yoon, T.-J.; Weissleder, R.; Lee, H. *ACS Nano* **2012**, *6*, 6821.
(12) Taboada, E.; Solanas, R.; Rodriguez, E.; Weissleder, R.; Roig, A. *Adv. Func. Mater.* **2009**, *19*, 2319.
(13) Chen, H.; Yeh, J.; Wang, L.; Khurshid, H.; Peng, N.; Wang, A. Y.; Mao, H. *Nano Res.* **2010**, *3*, 852.
(14) Maity, D.; Chandrasekharan, P.; Pradhan, P.; Chuang, K.-H.; Xue, J.-M.; Feng, S.-S.; Ding, J. *J. Mater. Chem.* **2011**, *21*, 14717.
(15) Liu, G.; Xie, J.; Zhang, F.; Wang, Z.; Luo, K.; Zhu, L.; Quan, Q.; Niu, G.; Lee, S.; Ai, H.; Chen, X. *Small* **2011**, *7*, 2742.
(16) Silva, A. K. A.; Di Corato, R.; Gazeau, F.; Pellegrino, T.; Wilhelm, C. *Nanomedicine* **2012**, DOI: 10.2217/nnm.12.40.
(17) Riedinger, A.; Leal, M. P.; Deka, S. R.; George, C.; Franchini, I. R.; Falqui, A.; Cingolani, R.; Pellegrino, T. *Nano Lett.* **2011**, *11*, 3136.
(18) Zeng, H.; Rice, P. M.; Wang, S. X.; Sun, S. H. *J. Am. Chem. Soc.* **2004**, *126*, 11458.
(19) Yu, W. W.; Falkner, J. C.; Yavuz, C. T.; Colvin, V. L. *Chem. Commun.* **2004**, 2306.
(20) Matsuoka, H.; Tanaka, H.; Hashimoto, T.; Ise, N. *Phys. Rev. B* **1987**, *36*, 1754.
(21) Matsuoka, H.; Tanaka, H.; Iizuka, N.; Hashimoto, T.; Ise, N. *Phys. Rev. B* **1990**, *41*, 3854.
(22) Gazeau, F.; Levy, M.; Wilhelm, C. *Nanomedicine* **2008**, *3*, 831.
(23) Baranov, D.; Fiore, A.; van Huis, M.; Giannini, C.; Falqui, A.; Lafont, U.; Zandbergen, H.; Zanella, M.; Cingolani, R.; Manna, L. *Nano Lett.* **2010**, *10*, 743.
(24) Porod, G. *Kolloid Z.* **1951**, *124*, 83.
(25) Zysler, R. D.; Fiorani, D.; Testa, A. M. J. *Magn. Magn. Mater.* **2001**, *224*, 5.
(26) Tronc, E.; Fiorani, D.; Nogues, M.; Testa, A. M.; Lucari, F.; D'Orazio, F.; Greneche, J. M.; Wernsdorfer, W.; Galvez, N.; Chaneac, C.; Mailly, D.; Jolivet, J. P. *Magn. Magn. Mater.* **2003**, *262*, 6.
(27) Song, H. M.; Kim, Y. J.; Park, J. H. *J. Phys. Chem. C* **2008**, *112*, 5397.
(28) Kechrakos, D.; Trohidou, K. N *Magn. Magn. Mater.* **2003**, *262*, 107.
(29) Trohidou, K.; Vasilakaki, M. *Acta Phys. Pol., A* **2010**, *117*, 374.
(30) Di Corato, R.; Quarta, A.; Piacenza, P.; Ragusa, A.; Figuerola, A.; Buonsanti, R.; Cingolani, R.; Manna, L.; Pellegrino, T. *J. Mater. Chem.* **2008**, *18*, 1991.
(31) Tromsdorf, U. I.; Bigall, N. C.; Kaul, M. G.; Bruns, O. T.; Nikolic, M. S.; Mollwitz, B.; Sperling, R. A.; Reimer, R.; Hohenberg, H.; Parak, W. J.; Forster, S.; Beisiegel, U.; Adam, G.; Weller, H. *Nano Lett.* **2007**, *7*, 2422.
(32) Martina, M. S.; Fortin, J. P.; Menager, C.; Clement, O.; Barratt, G.; Grabielle-Madelmont, C.; Gazeau, F.; Cabuil, V.; Lesieur, S. *J. Am. Chem. Soc.* **2005**, *127*, 10676.
(33) Pellegrino, T.; Manna, L.; Kudera, S.; Liedl, T.; Koktysh, D.; Rogach, A. L.; Keller, S.; Radler, J.; Natile, G.; Parak, W. J. *Nano Lett.* **2004**, *4*, 703.